

Article

Preliminary Investigation of the Remnants of Low-Latitude Glacial Activity on the Southeastern Margin of the Qinghai–Tibet Plateau

Yiwen Pan ^{1,2,3}, Shitao Zhang ^{3,*}, Jianping Chen ^{1,2}, Cheng Zhang ^{1,2} and Shuangshuang Wu ^{1,2}

¹ School of Earth Sciences and Resources, China University of Geosciences, Beijing 100083, China; panyw@email.cugb.edu.cn (Y.P.); 3s@cugb.edu.cn (J.C.); 3001210074@email.cugb.edu.cn (C.Z.); wss0805@163.com (S.W.)

² Beijing Key Laboratory of Development and Research for Land Resources Information, Beijing 100083, China

³ Faculty of Land Resources Engineering, Kunming University of Science and Technology, Kunming 650093, China

* Correspondence: zsx180329@163.com

Abstract: The formation of Quaternary glaciers represented a pivotal event in the climatic and geological history of the Tibetan Plateau. However, due to the scarcity of direct evidence for low-latitude glaciation, the timing and extent of late Quaternary glaciation on the Tibetan Plateau remain controversial. This study focuses on the Liangwang Mountains, which are located in the southeastern part of the Tibetan Plateau and has a maximum elevation of 2820 m, as the subject of investigation. Through a comprehensive application of glacial landform analysis, scanning electron microscopy (SEM)-based micromorphology analysis of quartz sand, and spore-pollen data analysis, we uncovered evident signs of glacial activity in this region during the Quaternary period. Our research identified typical glacial landforms such as cirques, U-shaped valleys, fluted moraines, and terminal moraines. Additionally, spore-pollen analysis revealed a high frequency of fir pollen, indicating cold climatic conditions during that time. Furthermore, the micromorphology analysis of quartz sand further corroborated the glacial origin of these deposits. Based on these combined findings, our study confirms that the Liangwang Mountains experienced glaciation during the Quaternary period, making them glacial relics at the lowest latitude currently known in mainland China. This discovery provides a valuable reference for understanding the paleoclimate and glacial history of the Tibetan Plateau and its surrounding regions.

Keywords: glacial geomorphology; penultimate glaciation; glacial sequences; Liangwang Mountains



Citation: Pan, Y.; Zhang, S.; Chen, J.; Zhang, C.; Wu, S. Preliminary Investigation of the Remnants of Low-Latitude Glacial Activity on the Southeastern Margin of the Qinghai–Tibet Plateau. *Sustainability* **2024**, *16*, 3492. <https://doi.org/10.3390/su16083492>

Academic Editor: Nemanja Tomić

Received: 27 February 2024

Revised: 13 April 2024

Accepted: 16 April 2024

Published: 22 April 2024



Copyright: © 2024 by the authors. Licensee MDPI, Basel, Switzerland. This article is an open access article distributed under the terms and conditions of the Creative Commons Attribution (CC BY) license (<https://creativecommons.org/licenses/by/4.0/>).

1. Introduction

The investigation of Quaternary environments and their evolution holds profound implications for human survival and has garnered significant scholarly attention [1,2]. A particularly important research topic is the study of Quaternary glaciers [3,4]. The Qinghai–Tibet Plateau, as the highest plateau in the world, is not only home to modern glaciers, but also hosts numerous ancient glacial relics in its hinterland and adjacent mountains [5–8]. These relics serve as valuable records of significant climatic changes that has occurred throughout the Quaternary period [9–11]. The southeastern Qinghai–Tibet Plateau is highly sensitive to Quaternary global climate change [12,13]. It is characterized by a strong monsoonal influence, distinct natural geographic vertical zonation, and noticeable topographic and climatic variation [14]. This region holds significant importance for the formation of monsoonal maritime glaciers. Evidence of a Quaternary climate is preserved in the glacial relics found at different altitudes and latitudes within the region [12,15]. These relics serve as valuable indicators of the ancient glacial systems' advancement and retreat during the Quaternary period.

To comprehend the relationship between the Quaternary climate, the uplift of the Tibetan Plateau, and global events in the southeastern Tibetan Plateau, numerous scholars have conducted studies on the glacial relics found in this area. They have explored the interplay between glacial development, climate, and tectonics [16,17]. Among the mountains on the southeastern edge of the Tibetan Plateau, the glacial relics provide the most valuable information for a detailed analysis of glacial development in relation to climate and tectonics [18–20]. Specifically, the glacial relics at lower latitudes exhibit highly sensitive climate response characteristics and offer more precise records of climate change during the Quaternary period [21]. However, many low-latitude glacial relics in the southeastern Tibetan Plateau have either been destroyed or remain undiscovered due to weathering and erosion. This limits our ability to analyze the coupling between glacial development, climate, and tectonics, and hinders our understanding of the timing and extent of late Quaternary glacial activity on the Tibetan Plateau. The Liangwang Mountains, which are the focus of this study, are located on the southeastern edge of the Tibetan Plateau and have an even lower latitude than the existing glacial relics in the southeastern part of the plateau. Consequently, the Liangwang Mountains represent the lowest-latitude glacial relics in mainland China. The study of these relics is not only crucial for investigating the coupling relationship between glacial development, climate, and tectonics, as well as the extent of Quaternary glaciation, but also aids in analyzing whether the glacial advancements on the Tibetan Plateau were triggered by temperature cooling or the increased moisture brought about by strong Indian summer winds.

To validate the occurrence of glacial development in the Liangwang Mountains during the Quaternary period, this paper examines the geomorphological characteristics of the region. The focus is placed on the microscopic morphological features of the quartz sand and spore powder present in sediments from the area of the Liangwang Mountains. Field geological surveys, geomorphological analyses, scanning electron microscopy experiments, and spore analysis experiments are employed to investigate glacial relics in the Liangwang Mountains.

The primary objectives of this study are as follows:

- (1) To establish the presence of Quaternary glacial activity in the Liangwang Mountains;
- (2) To determine the environmental conditions that facilitated glacier formation in this region;
- (3) To explore the factors contributing to glacial development in the Liangwang Mountains, considering its unique low-latitude location.

2. Materials and Methods

2.1. Study Area

The Liangwang Mountains region is situated on the southeastern margin of the Tibetan Plateau, southeast of Kunming city, Yunnan Province, China. It is located at the geographic coordinates of N 24°46′06.3″ and E 102°55′08.2″, with an elevation of approximately 2800 m above sea level. The mountains are encompassed by three prominent highland lakes: Dianchi Lake, Fuxian Lake, and Yangzonghai Lake (Figure 1). The study area is characterized by a predominantly elevated terrain, with the highest peak reaching 2820 m and the lowest altitude recorded at 2140 m, resulting in a maximum relative height difference of 680 m. The primary mountain range in the Liangwang Mountains region exhibits a predominant orientation towards the northeast, while the valleys within the mountain range predominantly follow a northeast to southwest direction. The area of the Liangwang Mountains is characterized by a secondary planation surface, featuring an overall steep terrain. Some areas have been subject to gully erosion, resulting in deeply incised terrain and steep slopes. The topographic slopes in the entire region range from 5 to 25 degrees, with certain localized areas exhibiting slopes exceeding 30 degrees.

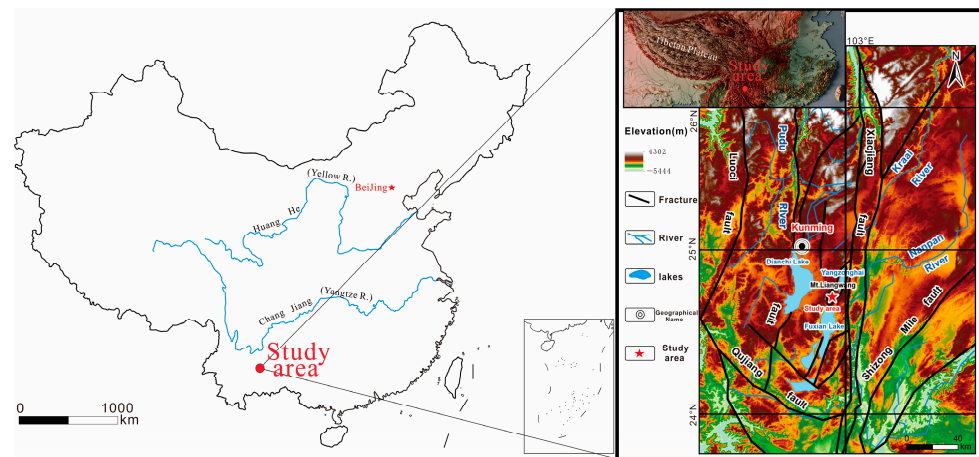


Figure 1. Study area location map.

The Liangwang Mountains are situated within the geotectonic context of the Yangzi–South China land mass area (V), the upper Yangzi ancient block (V-2), and the eastern margin of the Kunming depressional zone in the Kang–Dian basal fault zone (V-2-3). To the east of the area lies the western branch of the north–south Xiaojiang Fault, while the Pudu River Fault Zone borders it to the west. The tectonics of the area around the Liangwang Mountains are primarily influenced by the north–south-oriented Pudu River and Xiaojiang Fault.

2.2. Field Survey and Topographic Analysis

Geomorphological mapping is a well-established method that is used to study earth surface processes and landscape evolution in various environmental contexts [22]. In this study, we employed a combination of Google Earth image analysis, fieldwork, and indoor experimental analysis to determine the specific distribution characteristics of glacial landforms in the Liangwang Mountains.

To begin with, we developed a detailed expedition route using 1:50,000 topographic maps and Google Earth images. A month-long field trip was then conducted to investigate and analyze the macroscopic topography of the area around the Liangwang Mountains. During this field trip, we marked the distribution of glacial landforms on the 1:50,000 topographic map, labeled them, and collected samples from accumulations that exhibited the characteristics of glacial deposits. The sampling points YLQS01, YLQS02, YLQS03, and YLQS04 in the U-shaped valley area are located at a lateral moraine upstream of Yangliuqin. The thickness of the entire profile is approximately 6 m, and the sampling depth is 30 cm. Due to its special geographical location, this lateral moraine is less prone to alteration and destruction due water flowing through the central part of the valley at later stages, resulting in it being well preserved. The sampling points YLQX01 and YLQX02 are situated at a mixed deposit of ice and water downstream of Yangliuqin. The profile stands at approximately 5 m high, with a sampling depth of 20 cm. The sediment at this location consists of material from the upstream basal moraine of Yangliuqin that was transported and deposited here by river flow. In the Fengkoucun area, sampling points FK01 and FK02 are positioned at a lateral moraine adjacent to an eastern gully. The profile measures approximately 8 m in height, and the sampling depth is 50 cm. A prominent cirque has developed at the top of this gully, and the glacier flows down from the cirque, eroding the surface and forming a gully. Finally, based on the results of indoor experimental analysis, we identified three glacial deposits and mapped the distribution of glacial landforms in the Liangwang Mountains, using the 1:50,000 topographic map as a reference.

2.3. Scanning Electron Microscope Analysis of Quartz Sand

The use of scanning electron microscopy (SEM) is crucial for characterizing the morphology of quartz sand and deducing sediment transport modes and depositional environ-

ments [23–28]. Quartz sand, known for its high hardness, resistance to weathering, and stability, retains microscopic morphological features on its surface, which are formed by various transport forces. To determine whether the sediments in the Liangwang Mountains were deposited under glacial conditions, we analyzed the microscopic morphological characteristics of quartz sand particles using SEM. Initially, we conducted a field trip to the Liangwang Mountains and identified sediments that exhibited characteristics that were consistent with glacial accumulation. Samples were collected from different layers and passed through a 0.5 mm sieve. Each sample, weighing approximately 20 g, underwent organic matter removal via soaking in a 1:3 H₂O₂ solution. The reacted samples were then soaked in a 1:30 dilute HCl solution for 12 h. Subsequently, the samples were boiled on an electric hot plate until the gravel turned white. They were then rinsed with distilled water, and dried under a microscope in a drying oven set to 40 °C. For each sample, 50 grains of quartz sand with particle sizes ranging from 0.2 to 0.5 mm were selected, uniformly bonded to the carrier table, and coated with a layer of conductive gold film in a vacuum coater in order to perform microscopic (The manufacturer of the thermo scientific quattro s scanning electron microscope equipment is Thermo Fisher Scientific, and it was purchased through Beijing, China) observation.

Referring to previous studies [25,29], we categorized 39 different depositional environments into typical micromorphological features (Table 1). These features were further grouped into three categories: shapes of quartz sand, mechanical features, and chemical features. A statistical table was created to determine the total frequency of the micromorphological features associated with each depositional environment. After SEM analysis, samples that did not exhibit the typical microformation features of glacial environments were excluded. The remaining samples, displaying features characteristic of glacial environments, were plotted as scatter plots.

Table 1. Quartz sand morphological characteristics.

Shape of quartz sand	Roundedness	13: well-rounded; 14: round; 18: subrounded; 25: subangular; 34: multangular; 35: pointed
	Edge shape	15: abraded edge; 17: subrounded edge; 24: subangular ridge; 32: ridge erosion; 33: sharp-edged ridge
	Relief	16: low relief; 23: moderate relief; 31: high relief
Mechanical		10: sinuous ridge; 11: folded cleavage planes; 12: dish-shaped pits; 19: subaqueous polish; 20: small impact crater; 21: straight grooves; 22: V-shaped gouges; 26: small shell-shaped fragments; 27: adhering fragments; 28: fractures; 29: parallel striations; 30: deep impact crater; 36: terraces; 37: parallel cleavage planes; 38: medium-sized shell-shaped fractures; 39: large shell-shaped fractures
Chemical		1: flakey exfoliation; 2: silica crystallization; 3: amorphous silica precipitation; 4: siliceous film; 5: siliceous scales; 6: siliceous sphere; 7: honeycomb etching surface; 8: oriented etch pits; 9: pits and grooves

2.4. Sporopollen Analysis

Sporopollen is a valuable indicator of climate response, as different climates support the growth of distinct plant types. The preservation potential of palynology makes it an ideal tool for reconstructing paleoclimates [30,31]. Sporopollen analysis employs the traditional method of sporopollen stratigraphy, which involves assessing the composition and abundance of various genera and species within the four major plant groups of trees, herbs, shrubs, and ferns based on the natural classification system. This analysis aims to stratigraphically divide and compare layers, determine the ancient vegetation cover, and reconstruct the ancient climate. By quantifying the spore content of each species, we can conduct quantitative research on ancient vegetation and climates. Utilizing sporopollen analysis data, we established three quantitative models: spore-pollen vegetation types, spore-pollen climatic zones, and spore-pollen humidity levels. In order to assess whether the paleoclimatic conditions prevailing

during the development of glaciers in the Liangwang Mountains were consistent with the conditions required for glacier formation, we conducted a sporopollen analysis of sediments collected from the Liangwang Mountains. A total of 26 samples were collected and processed, following the following procedure: crushing and weighing the samples; treating them with NaOH (10%), 10% HCL, and HF; sieving them using a 40~50 W ultrasonic shaker and a 5 μm sieve; and microscopic observation.

3. Results

3.1. Geomorphological Features of the Glacier in the Liangwang Mountains

To determine the distribution of glacial relics in the area around the Liangwang Mountains, we utilized a comprehensive analysis method, combining fieldwork and indoor experiments. The summit area and the source of the valley in the Liangwang Mountains exhibit numerous glacial erosion landforms, including cirques, U-shaped valleys, fluted moraines, and moraine topography. The western and eastern faces of the main peak of the Liangwang Mountains (2820 m) predominantly present glacial cirques (Figure 2), with a general altitude distribution of around 2600 m. However, it is important to note that the Liangwang Mountains lie within the North Subtropical Low-Latitude Plateau Monsoon Climate Zone, characterized by distinct wet and dry seasons. Moreover, the peak region of the mountains primarily consists of limestone, rendering it susceptible to erosion and damage caused by rainfall and runoff. Consequently, some glacial cirques and ridges have undergone erosion and destruction, while the main prominent features have been preserved (Figure 3). To further analyze the glacial cirques in the area of the Liangwang Mountains, we calculated the flatness index using a 1:50,000 topographic map of Chengjiang County and field measurements. The calculated flatness index of these glacial cirques ranged from approximately 1.80 to 3.54.

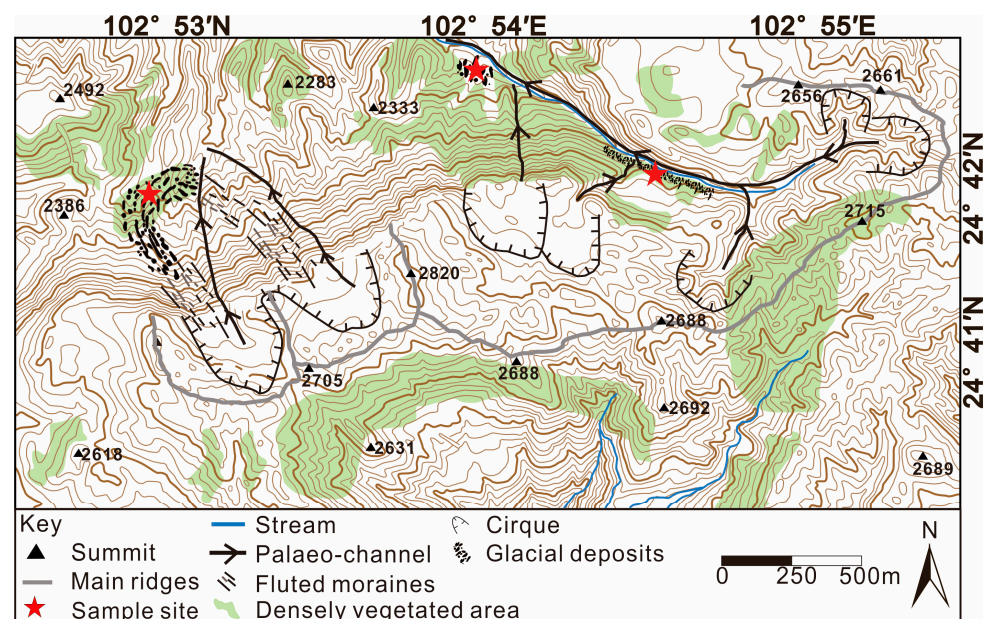


Figure 2. Glacial geomorphology of the Liangwang Mountains.

There are U-shaped valleys (Figure 4) located to the northeast of the main peak of the Liangwang Mountains. These valleys exhibit open and relatively flat bottoms, display steep valley slopes, and are covered with contemporary vegetation. The valleys measure 40 m in width and stretch over a length of 1000 m, with a northwest orientation. Most of these valleys have been impacted by modern gully erosion, resulting in the preservation of only partial glacial deposits in the central and lower portions. Using a power-law function model, we calculated the b-index of valleys at different elevations in the area around the

Liangwang Mountains. The b-index fluctuates within the range of 1.681 to 2.057 for the valleys of different elevations in the area around the Liangwang Mountains.

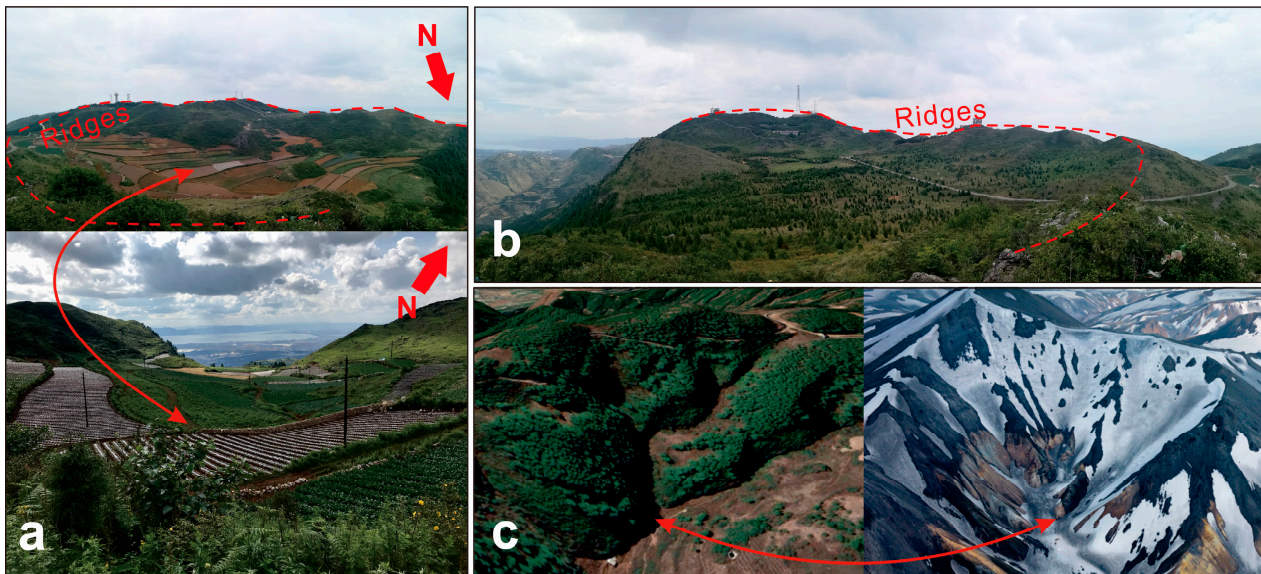


Figure 3. Cirques ((a,b) are relatively typical cirques in the area around Liangwang Mountains, where the mountain ridges have suffered severe erosion and damage. (c) is a cirque that has suffered significant damage, and we have made attempts to restore its original geomorphology).

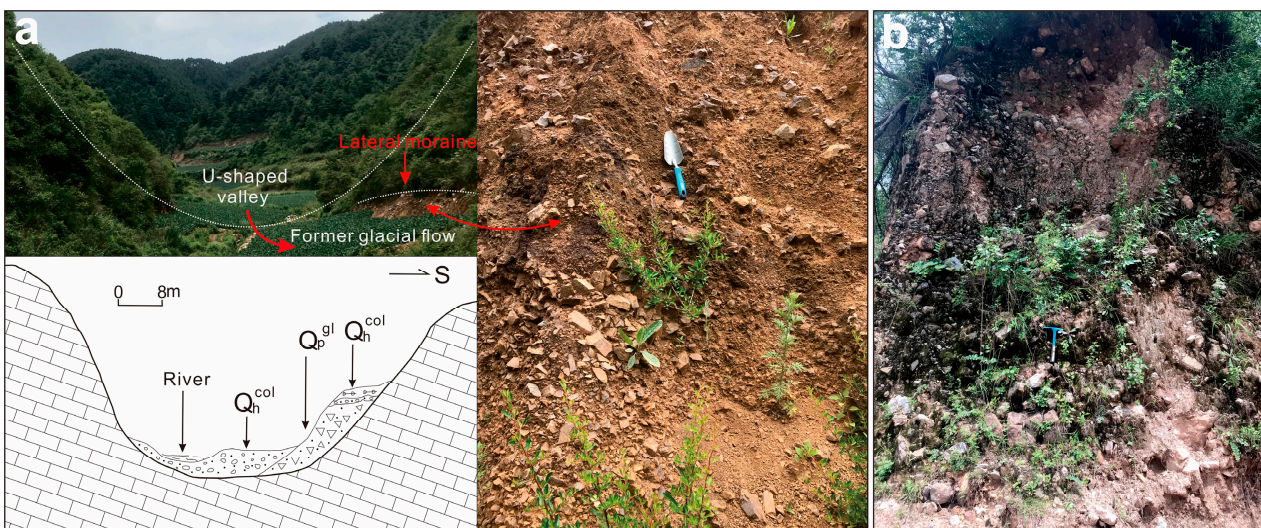


Figure 4. U-shaped valleys and glacial deposits ((a) is a U-shaped valley with a lateral moraine located within it. (b) is a terrace formed by the transportation and accumulation of glacial deposits by flowing water in the upstream area).

Within the area around the Liangwang Mountains, there are three distinct sets of moraine assemblages that represent remnants from the same ice age. The first set consists of lateral moraine landforms found within the U-shaped valleys of the Liangwang Mountains (Figure 4a). These lateral moraines exhibit exposed moraine rocks, primarily composed of angular or subangular limestone. The rocks display a mixed size distribution, lack sorting, and show signs of weak weathering, which are characteristics of moraine rocks formed through glacial action (Figure 5d,e).

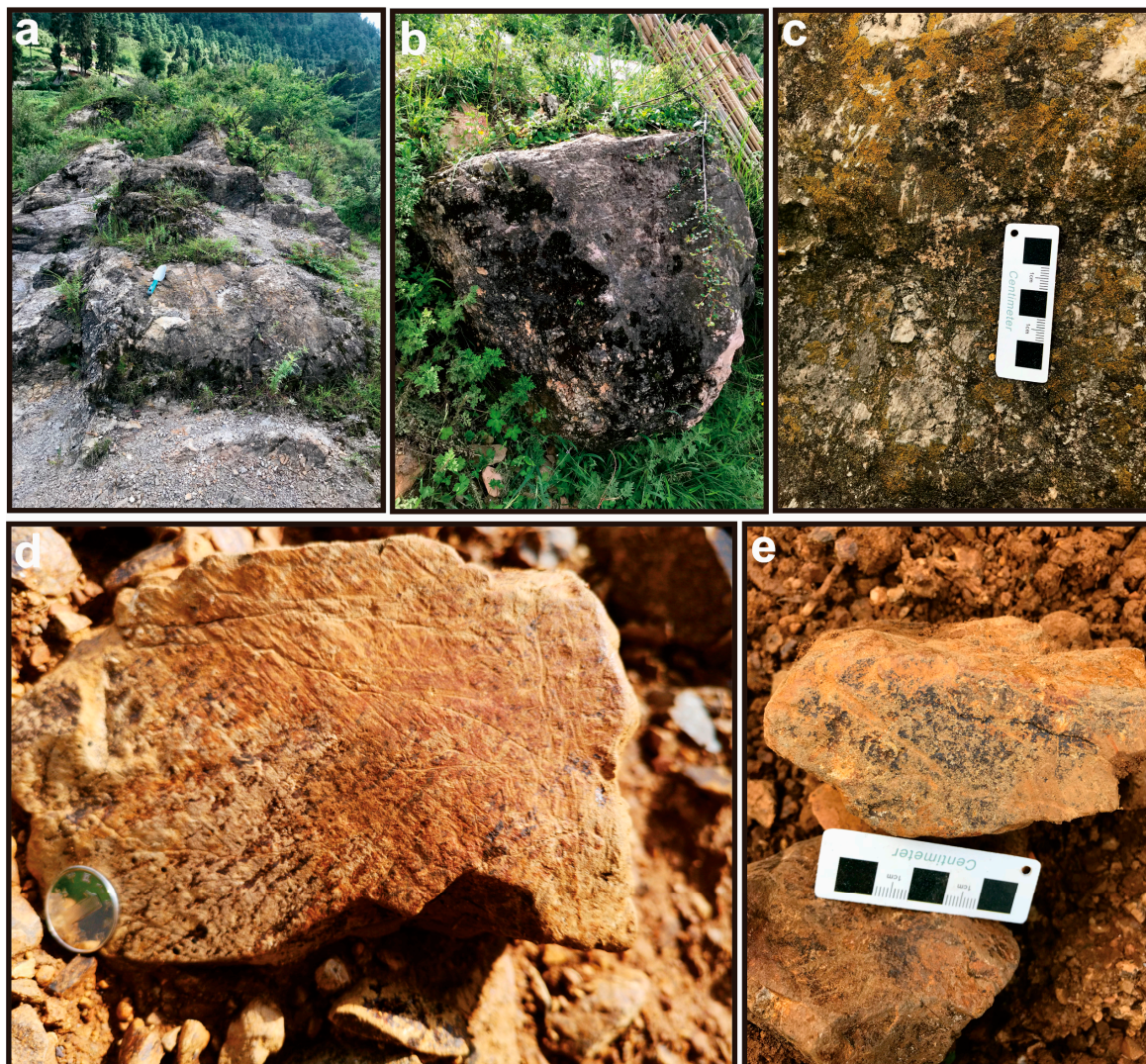


Figure 5. Moraine ((a) refers to boulders distributed on the lateral moraines of Fengkou village. (b,c) are characteristics of individual boulders. (d,e) are moraine rocks found in the lateral moraines within the U-shaped valley, exhibiting typical glacial features).

The second set of lateral moraines is located in the eastern part of Fengkou village, adjacent to the washout gully. These landforms are covered by modern plants, with boulders scattered across their surface (Figure 5a,b). The predominant lithology is dolomite, and the rocks within this set have a diameter of 1–2 m and show a high degree of weathering. They are distributed in a continuous band along the lateral moraine landform, and some gravel surfaces exhibit small rub marks in the same direction (Figure 5c).

The third set of glacial deposition is represented by an ice-water terrace (Figure 4b). This feature comprises moraine deposits that originate from the central upstream part of Yangliuqin. It formed through the transportation and accumulation of water subsequent to the initial glacial activity. As a result, the terrace retains certain moraine characteristics while also displaying traits associated with flowing water. The accumulated terrace primarily consists of limestone gravel, which is highly prone to erosion by flowing water. Consequently, during the transportation and accumulation process, prominent features were eroded and removed by flowing water.

3.2. Characterization of the Quartz Particle Morphology

Through extensive sampling and rigorous indoor experimental analysis, we identified three distinct locations in the area around the Liangwang Mountains that consistently

displayed the characteristics of glacial deposits. These sites included the upstream lateral moraine (YLQS) of Yangliuqin, the downstream glaciofluvial terrace (YLQX) of Yangliuqin, and the eastward lateral moraine (FK) near Fengkou village.

The majority of quartz sand grains collected from glacial sediments in the area around the Liangwang Mountains exhibited pointed, subangular, and multangular shapes. Among the three micromorphological features (well-rounded, round, and subrounded), subrounded grains occurred sporadically and with a very low frequency. The analysis of edge-shape statistics revealed a high frequency of subangular ridges and sharp-edged ridges, while ridge erosion and subrounded edges were less frequent, and no samples with abraded edges were observed. The relief morphology statistics indicated that quartz sand particles with high relief and depths greater than $1\ \mu\text{m}$ had the highest frequency, followed by particles with moderate relief and depths between $0.5\ \mu\text{m}$ and $1\ \mu\text{m}$, which also had a relatively higher frequency. Quartz sand particles with low relief and depths less than $0.5\ \mu\text{m}$ had a lower frequency. Overall, the selected quartz sand particles in this study predominantly exhibited pointed subangular ridges with moderate-to-high relief (Figure 6a). The observation of the selected quartz sand grains revealed their lack of overall rounding and prominent angles, indicating minimal transportation after detachment from the parent rock. This suggests that the glacier in the area around the Liangwang Mountains was relatively small in scale and had a short transportation distance.

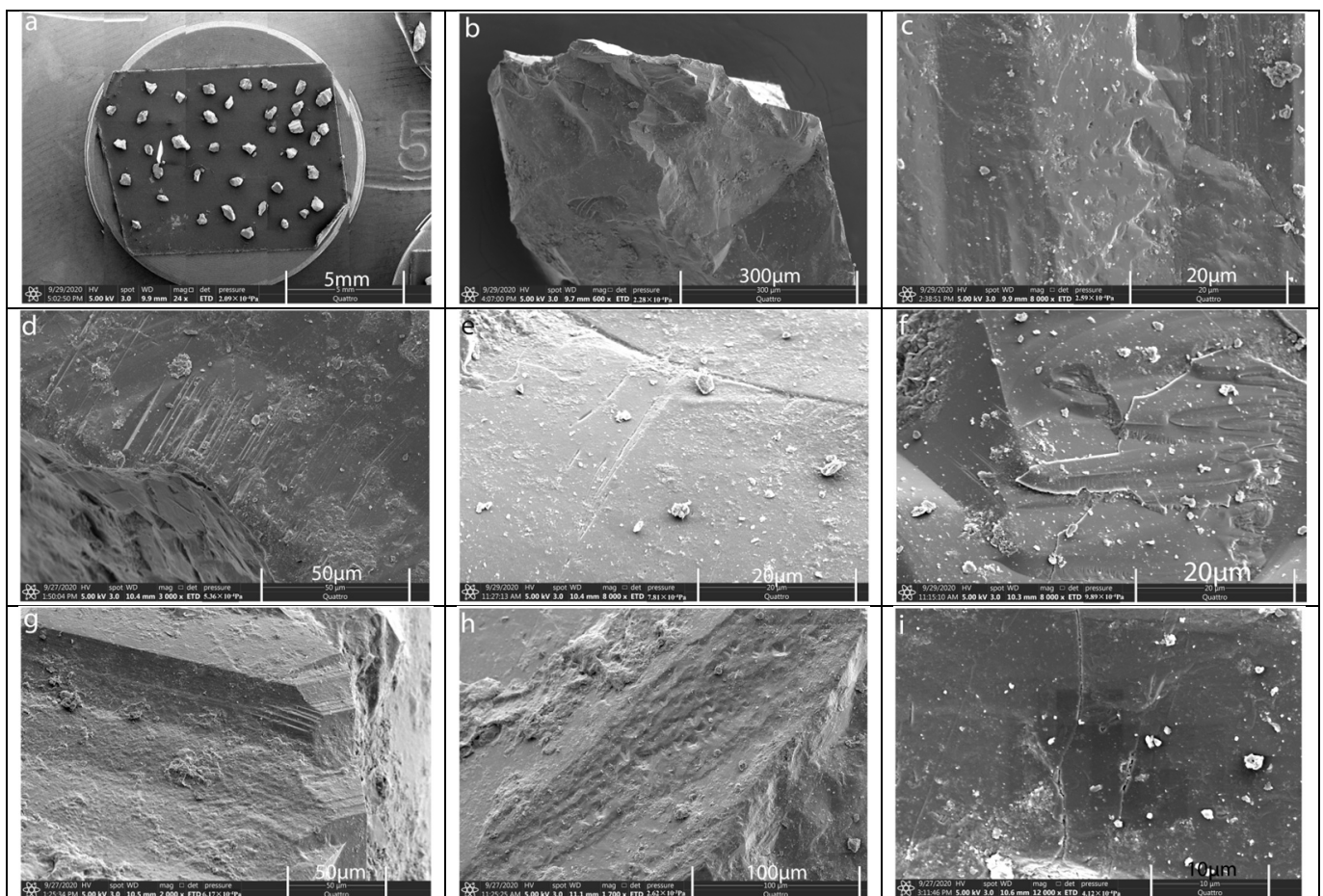


Figure 6. Typical mechanical characteristics of the Liangwang Mountains quartz sand, as determined via SEM analysis ((a) is the shape of some quartz sand particles; (b) represents the shell-shaped fractures; (c) is V-shaped gouges and; (d,e) is parallel striations; (f) shows adhering fragments and parallel striations; (g) represents terraces; (h) is a small impact crater; and (i) represents fractures).

In this study, various mechanical features were observed on the surfaces of the selected quartz grains, including shell-shaped fractures of different morphologies (Figure 6b), V-shaped gouges (Figure 6c), parallel striations (Figure 6d,e), adhering fragments (Figure 6f), terraces (Figure 6g), small impact craters (Figure 6h), and fractures (Figure 6i). The frequencies of these micromorphological features were calculated, revealing that small shell-shaped fractures with lengths less than 20 μm occurred at a frequency ranging from 10% to 40%, with an average frequency of 29%. Medium-sized shell-shaped fractures with lengths between 20 μm and 40 μm occurred at a frequency ranging from 8% to 30%, with an average frequency of 18%. Large shell-shaped fractures with lengths greater than 40 μm occurred at a frequency ranging from 10% to 40%, with an average frequency of 22%. The occurrence of terraces on the quartz grain surfaces was relatively low, ranging from 0% to 10%, with an average frequency of 4%. This limited occurrence suggests a restricted scale of glacial development in the Liangwang Mountains, resulting in weaker forces being exerted by the ice body on the quartz sand surface. Higher frequencies of V-shaped gouges and small impact craters, which are characteristic morphological features of a flowing water environment, were observed in samples YLQX01 and YLQX02 compared to samples YLQS01, YLQS02, YLQS03, YLQS04, FK01, and FK02. The frequencies of V-shaped gouges and small impact craters in samples YLQX01 and YLQX02 were 22–28%, while their frequencies were lower in the remaining samples. This indicates the presence of flowing water in the depositional environment, specifically in samples YLQX01 and YLQX02. In this experiment, no underwater polished surfaces were found on the surfaces of the collected quartz grains. Only V-shaped gouges were observed on some of the quartz sand grains, indicating the presence of strong flowing water during deposition. However, the activity time was sufficiently short to prevent the formation of underwater polished surfaces.

The presence of iconic micromorphological features closely associated with glaciation, such as parallel striations, adhering fragments, and fractures, is considered to be a representative indicator of glacial processes. The statistical analysis conducted in this study revealed a high frequency of these micromorphological features at all three sampling sites, suggesting the involvement of glaciation in the sediment transport process. Parallel striations, which are linear or curved marks on the quartz surface, serve as important markers for identifying glaciation [25,29]. These striations are formed through the mutual friction between quartz grains and display similarities to terraces and parallel cleavage planes. After careful screening, it was observed that the quartz grains with surface rub marks accounted for 8% to 36% of the samples, with an average frequency of 22%. Adhering fragments, generated by the pressure of overlying glacial ice, are typical microforms observed in the quartz sand within glacial environments. These fragments were present in all eight samples, with a frequency ranging from 14% to 30% and an average frequency of 21%. Fractures that are often considered indicative of glacial action were also observed to varying degrees on the surfaces of quartz grains during the SEM analysis conducted by several scholars. In this experiment, fractures were present with a frequency ranging from 6% to 22%, and an average frequency of 13%.

The frequencies of the different microformation features of varying origins were counted using the environmental particle percentage method (Figure 7). It was found that the total frequency of microformation features related to glacial processes was higher than that associated with flowing water and wind processes. Although some samples showed environmental signs that suggested a contribution from flowing water, their frequency was relatively low, indicating a shorter duration of water involvement during deposition. Therefore, SEM analysis of quartz sand in the area around the Liangwang Mountains indicated that the sediments were formed in a glacial or glaciofluvial environment.

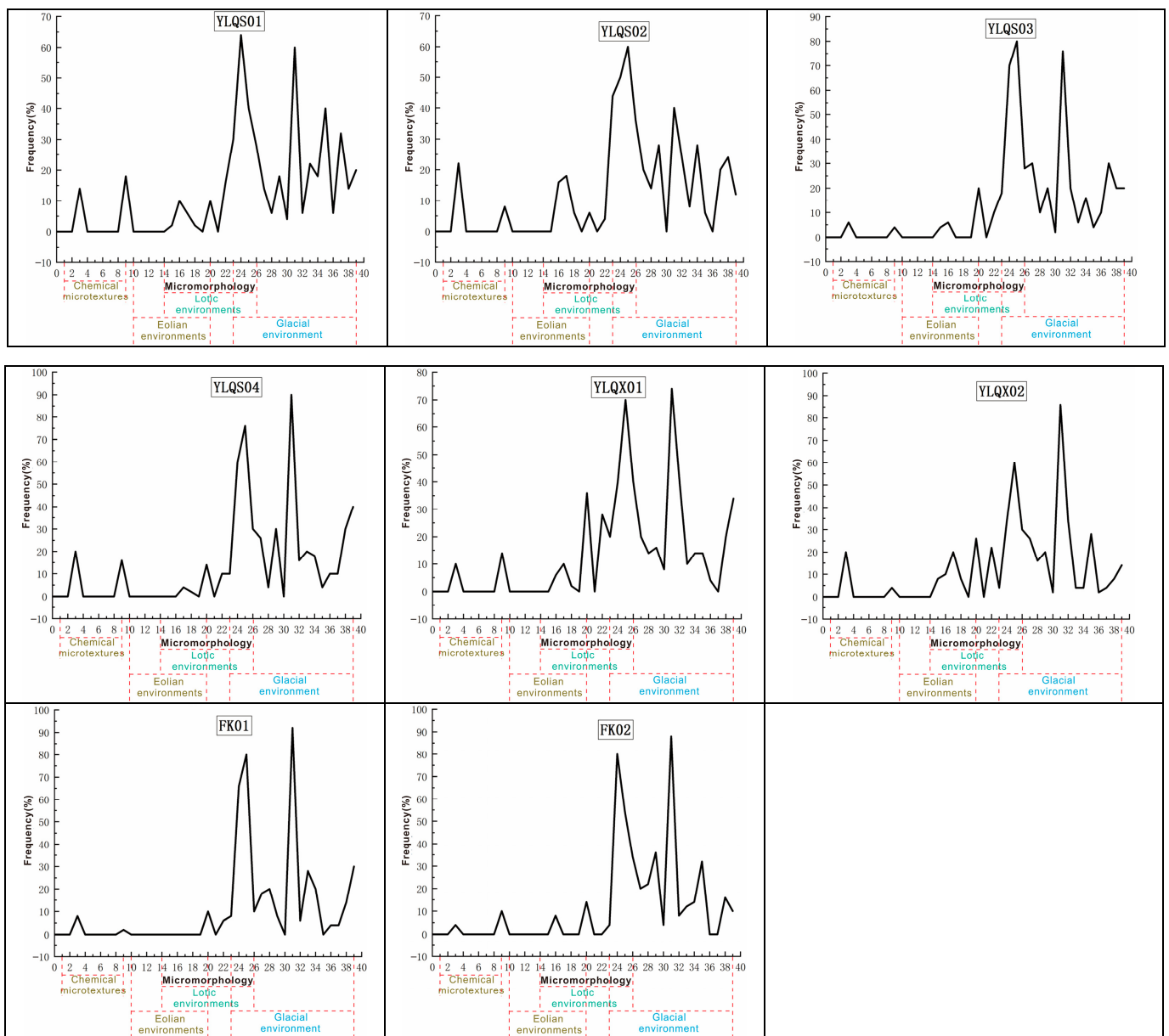


Figure 7. Scatter diagram of quartz sand micromorphological features in the area around the Liangwang Mountains.

3.3. Palynological Characterization

A total of 2 topsoil sporopollen samples were collected from the Liangwang Mountains. In these samples, a total of 1257 plant spore particles were counted, with 486 particles found in sample LWS01 and 771 particles identified in sample LWS02. Overall, 14 families (genera) were identified, including 6 families (genera) of woody plants, 3 families (genera) of herbaceous plants, and 5 families (genera) of ferns. The six main woody plant types identified were *Pinus*, *Alnus*, *Castanopsis*, *Quercus*, *Rhododendron*, and *Myrsine*. The three main types of herbaceous plants were *Gramineae*, *Artemisia*, and *Bidens*. The five main types of ferns identified were *Pteris*, *Pyrrosia*, *Polypodiodes*, *Humata*, and *Hicriopteris*. This study analyzed topsoil sporopollen samples from the Liangwang Mountains via comparative study with sporopollen from glacial sediments.

A total of 16 samples, labeled 1 to 16, were collected from the upstream Yangliuqin moraine section, and a total of 10,403 spores were counted. Among these spores, 946 were counted in samples 1 and 2, 1365 were counted in samples 3 and 4, 1466 were counted

in samples 5 and 6, 1287 were counted in samples 7 and 8, 880 were counted in samples 9 and 10, 1034 were counted in samples 11 and 12, 2403 were counted in samples 13 and 14, and 1022 were counted in samples 15 and 16. In this experiment, a total of 29 families (genera) of spore pollen were identified, including 13 families (genera) of woody plants, 7 families (genera) of herbaceous plants, and 9 families (genera) of ferns. The main woody plant types identified were *Pinus*, *Alnus*, *Castanopsis*, *Quercus*, *Cyclobalanopsis*, *Betulaceae*, *Abies*, *Picea*, *Tsuga*, *Albizia*, *Rhododendron*, *Myrsine*, and *Lonicera*. The main herbaceous plant types were *Gramineae*, *Artemisia*, *Chenopodium*, *Megacarpaea*, *Caryophyllaceae*, *Compositae*, and *Bidens*. The main fern types were *Pteris*, *Pyrrosia*, *Polypodiaceae*, *Polypodiodes*, *Humata*, *Athyrium*, *Lycopodium*, *Onychium*, and *Hymenophyllum*.

Based on the presence or absence of *Abies* in each layer of the profile, this study divides the upstream Yangliuqin moraine profile into two spore-pollen combination sections (Figure 8).

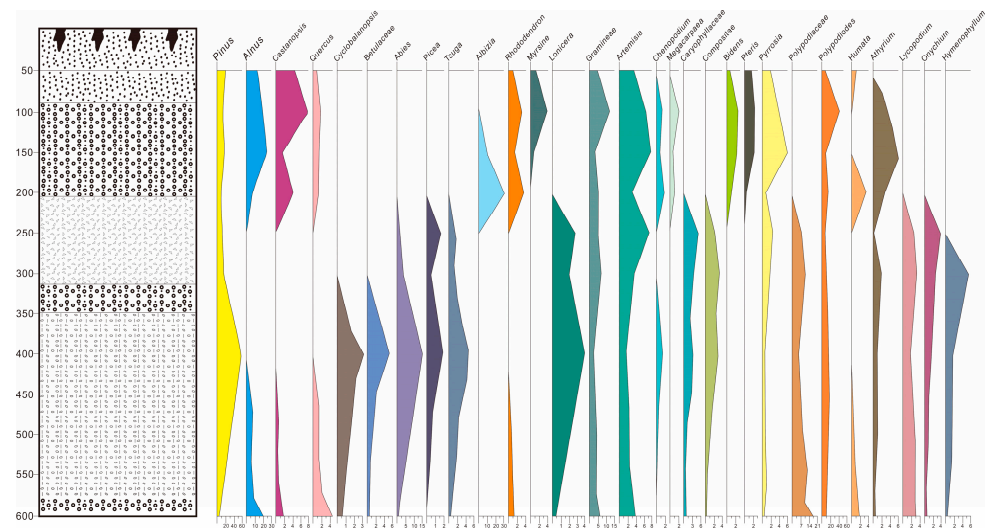


Figure 8. Spore-pollen count in the Yangliuqin upstream lateral moraine profile.

Section 1 of the spore-pollen count includes samples 1 to 5, with woody plant spores accounting for 55% to 76% of the material tested. The main species in this section are *Pinus*, *Alnus*, *Castanopsis*, *Quercus*, *Albizia*, *Rhododendron*, and *Myrsine*. Herbaceous plant spores account for 10% to 22%, including *Gramineae*, *Artemisia*, *Chenopodium*, *Megacarpaea*, and *Bidens*. Fern spores make up 8% to 19% of the spores, mainly *Pteris*, *Pyrrosia*, *Polypodiodes*, *Humata*, and *Athyrium*. This characteristic sporophyte assemblage indicates a mixed coniferous forest landscape in a warm and humid climate.

Section 2 of the spore-pollen count includes samples 6 to 18, with woody plant spores accounting for 47% to 85% of spores. The main species in this section are *Pinus*, *Cyclobalanopsis*, *Betulaceae*, *Abies*, *Picea*, *Tsuga*, and *Lonicera*. Herbaceous plant spores account for 5% to 25% of the total, including *Gramineae*, *Artemisia*, *Chenopodium*, *Caryophyllaceae*, and *Compositae*. Fern spores make up 8% to 32% of the spore powder, mainly *Pyrrosia*, *Polypodiodes*, *Polypodiodes*, *Athyrium*, *Lycopodium*, *Onychium*, and *Hymenophyllum*. *Abies* appears frequently in this spore-pollen section, reaching a maximum of 12.3% in the profile. *Alnus*, *Quercus*, and *Castanopsis* appear in lower concentrations in the early stage and gradually disappear in the late stage. The spore-pollen content of ferns gradually increases, reaching a maximum of 32%. These findings suggest a coniferous forest landscape under a cold temperate and humid climate. The main spores found in the moraine layers of the Liangwang Mountains include *Pinus*, *Cyclobalanopsis*, *Betulaceae*, *Abies*, *Picea*, *Tsuga*, *Lonicera*, *Gramineae*, *Artemisia*, *Chenopodium*, *Caryophyllaceae*, *Compositae*, *Pyrrosia*, *Polypodiaceae*, *Polypodiodes*, *Athyrium*, *Lycopodium*, *Onychium*, and *Hymenophyllum*.

Based on the analysis of topsoil spore powder characteristics in the Liangwang Mountains, fir (*Abies*) is no longer present in the area around the modern Liangwang Mountains.

However, *Abies* appears frequently in certain moraine layers, with its content reaching as high as 12.3%. This indicates that a significant amount of fir was growing in the Liangwang Mountains during that period. Presently, fir predominantly grows in the Yulong Mountains at an altitude of approximately 3800 m. Considering the vertically decreasing temperature rate of 0.6 °C at the same latitude, the average annual temperature in the area around the modern Liangwang Mountains is 11.7 °C. In contrast, the average annual temperature in the area around the Liangwang Mountains during that time was approximately 2 °C. This analysis of the paleoclimatic background suggests that the Liangwang Mountains possessed the suitable climatic conditions for glacial development during that period.

4. Discussion

4.1. Ice Age Discussion

The modern theoretical equilibrium line is determined using three calculation methods: a method using the maximum precipitation zone and empirical curve relationship (MPC), a method using the maximum precipitation zone with a statistical formula (MPF), and a method using weather station precipitation and an empirical formula (WPF) [32,33]. In this study, the modern theoretical equilibrium lines of the Liangwang Mountains were reconstructed using three methods: MPC, MPF, and WPF. These methods relied on meteorological data from the Chenggong weather station and reference data tables of equilibrium lines from typical glaciers [34].

Table 2 presents the modern theoretical equilibrium line of the Gongwang Mountains, which is approximately 4488 m. During the penultimate ice age, the equilibrium line of the Gongwang Mountains dropped to an altitude of around 1400 m [35,36], suggesting that the ancient equilibrium line of the Gongwang Mountains during that period was approximately 3000 m. Considering that the Liangwang Mountains share a similar climatic environmental background with the Gongwang Mountains as they are both located in the southeastern edge of the Qinghai–Tibet Plateau and the middle Yunnan Basin, we calculated the ancient equilibrium line of the Liangwang Mountains based on the maximum decline of 1400 m observed in the penultimate ice age. The calculated ancient equilibrium line of the Liangwang Mountains during the penultimate ice age was approximately 2800 m, which is close to the highest elevation of the Liangwang Mountains, which is only 2820 m. However, it is important to note that the modern theoretical equilibrium lines calculated in this study do not take into account other factors, and that the elevation of the weather station can affect the accuracy of the calculations. Based on the data collected in and presented Table 2, it can be concluded that the modern theoretical equilibrium lines of the Liangwang and Gongwang Mountains, both located in the central Yunnan Basin, are not equal. Additionally, the calculated modern theoretical equilibrium lines tend to be higher than the actual equilibrium lines, and the elevation of the weather station in proximity to the mountain peak affects the accuracy of the modern theoretical snow line value. Thus, the modern theoretical equilibrium line of the Liangwang Mountains is lower than that of the Gongwang Mountains, with a larger magnitude of difference. Moreover, the data used in this study are provided by the Chenggong meteorological station, and there is no meteorological station at the top of the Liangwang Mountains. According to relevant research, the precipitation measured at the bottom of the mountains is significantly lower than the precipitation measured on the mountains [37]. Combining these factors, it is likely that the modern theoretical equilibrium line of the Liangwang Mountains has an error of several hundred meters, indicating that the height of the ancient equilibrium line of the Liangwang Mountains during the penultimate ice age was lower than the current elevation of the Liangwang Mountains.

The penultimate ice age witnessed the most significant cooling in the southeastern edge of the Tibetan Plateau, resulting in the largest decline in the equilibrium line. In contrast, the decline during the last ice age was much smaller. Previous glacier research on the Qinghai–Tibet Plateau and its marginal mountains indicated that glacial development during the antepenultimate ice age, also known as the Zhong-lianggan ice age,

was primarily concentrated in the inner region of the Qinghai–Tibet Plateau. It was only during the penultimate ice age that glacial development gradually spread to the plateau’s edge [16,38,39].

Table 2. The altitude, summer temperature and precipitation at ELAs using different methods.

Method					MPC	MPF	WPF
Mountain Range	Height of Weather Station (m)	Weather Station June to August Temperature (°C)	Average Annual Precipitation at Meteorological Stations (mm)	Actual Equilibrium Line Height (m)	Theoretical Equilibrium Line Height (m)	Theoretical Equilibrium Line Height (m)	Theoretical Equilibrium Line Height (m)
Altai	1900	11.9	664	3320	3688	3750	3873
Tianshan	3539	4.3	454	4056	4239	4294	4365
Baima	4292	5.1	807.1	4800	4867	4942	5054
Yulong	2393	17.7	950	4800	5026	5076	5176
Luoji	2640	15.8	956		4940	5005	5103
Qianhu	3276	12.9	849.8		5134	5206	5312
Cangshan	1990	19.8	1054		4905	4980	5068
Gongwang	3900	6.8	1570		4488	4558	4553
Yushan	3845	7.4	3054		4361	4328	3953
Liangwang	1906	16.1	1100		4256	4262	4341

Given the proximity of the Liangwang Mountains to the Kunming Basin, Quaternary global cooling led to glacial development in the Liangwang Mountains, which could have influenced the Kunming Basin. Borehole studies conducted in different areas of the Kunming Basin revealed a higher occurrence of *Abies* in the Quaternary strata, peaking at 110,000 years, indicating an unprecedented flourishing of fir during this period [40,41]. In this study, we analyzed the presence of *Abies* in the glacial sediments of the area around the Liangwang Mountains and compared it with that of the Kunming Basin (Figure 9). The figures show that the presence of *Abies* in the boreholes of different areas in the Kunming Basin reached its peak at 110,000 years, while *Abies* in the moraine layer of the Liangwang Mountains peaked at a depth of approximately 4 m. This suggests that the age of this moraine layer is likely around 110,000 years, corresponding to the penultimate ice age.

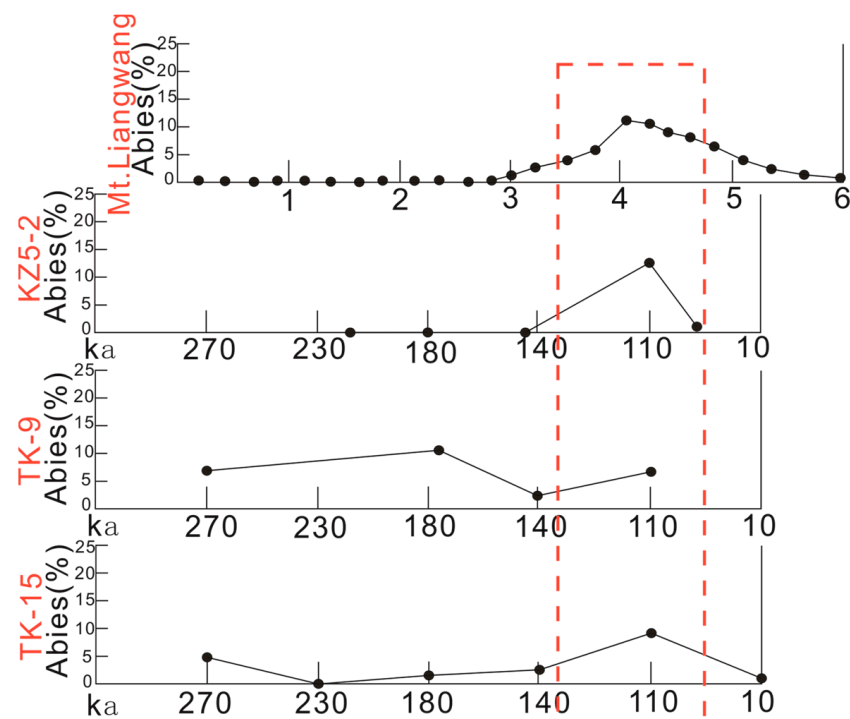


Figure 9. Comparison of the *Abies* spore powder content between different boreholes in the Kunming Basin and Liangwang Mountain.

In summary, from the perspective of the both the equilibrium line and sporulation, only glaciers are likely to have developed in the Liangwang Mountains during the penultimate ice age.

4.2. Why Did Glaciers Develop in the Liangwang Mountains?

The Quaternary ice age climate had a significant impact on the Qinghai–Tibet Plateau and its marginal mountains, resulting in the development of glaciers at different times on different mountains [38,41,42]. Comparing the ice age series of these mountain glaciers can provide insights into the factors contributing to their formation. Figure 10 shows a comparison of the ice age series of mountains in the southeastern Tibetan Plateau. It reveals that the Yulong and Luoji Mountains have the longest ice age history. These mountains began developing glaciers in the early Kunlun ice age around, at 700 ka B.P., while neighboring mountains such as Cangshan, Gongwang, Qianhu, and Liangwang Mountains did not have glaciers during that time. Despite the current altitudes of Cangshan, Gongwang, and Qianhu Mountains being similar to those of the Luoji Mountains, only the Yulong and Luoji Mountains had glaciers during the Kunlun ice age [43,44]. This suggests that tectonic movements likely played a significant role in the contrasting ice age histories under similar climatic conditions [45].

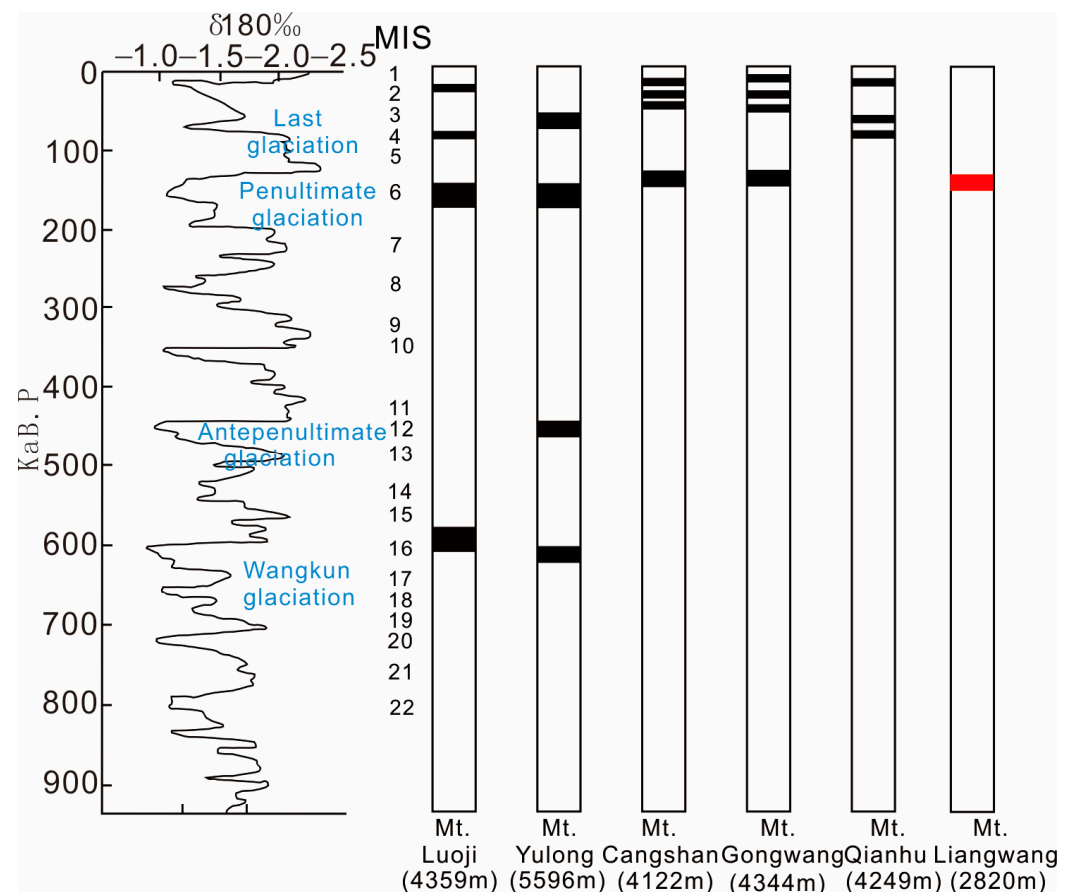


Figure 10. Comparison of the mountain ice age series in the southeastern Qinghai–Tibet Plateau.

The uplift of the Tibetan Plateau can be divided into three stages: the early “Qinghai–Tibetan Movement” from 3.6 to 1.7 Ma, the middle “Kunlun–Yellow River Movement” from 1.1 to 0.6 Ma, and the late “Republican Movement” since 0.15 Ma [43,46,47]. The Yulong Snow Mountains and the Luoji Mountains experienced the earliest development of the Kunlun ice age glaciers at around 700 ka B.P., likely due to the “Kunlun–Yellow River Movement”, which led to the significant uplift of the Tibetan Plateau. The surrounding mountains around the Qinghai–Tibet Plateau also underwent uplift, but with different

uplift rates due to varying fracture controls. The uplift rates of the Yulong Mountains and Luoji Mountains were much higher compared to those of the neighboring mountains [48]. Consequently, the Yulong and Luoji Mountains were the first to rise above the equilibrium line, allowing the development of glaciers during the Kunlun ice age. On the other hand, the Cangshan, Gongwang, Qianhu, and Liangwang Mountains were also affected by the Kunlun–Yellow River Movement and experienced uplift, but their uplift rates differed due to the influence of different fracture controls. However, these mountains did not reach the elevation of the equilibrium line and did not develop glaciers [34,49].

With the Republican Movement (since 0.15 Ma), as the strong uplift of the Tibetan Plateau entered a new phase, the southeastern part of the plateau experienced a notably colder period at around 0.15 Ma [12]. During this period, the equilibrium line of mountain glaciers dropped significantly, and mountains such as Gongwang, Cangshan, and Liangwang, which initially failed to reach the equilibrium line, were uplifted above it. As a result, these mountains began developing glaciers during the penultimate ice age.

During the penultimate ice age, the glacial development pattern in southeastern Tibet reached its peak [41,50]. Glaciers developed in the Cangshan, Gongwang, and Liangwang Mountains during this period. However, the Qianhu Mountains only experienced glacial development during the last ice age. The equilibrium line of the Gongwang Mountains dropped to approximately 3000 m during the penultimate ice age, whereas the current elevation of the Liangwang Mountains is only 2820 m. Based on the distribution characteristics of cirques in the Liangwang Mountains, the estimated equilibrium line during the penultimate ice age was 2600 m, disregarding tectonic uplift. Thus, there was a difference of several hundred meters in the equilibrium lines between these two mountain ranges during the penultimate ice age. These differences indicate that glacial development is not only influenced by tectonics, but also by other factors. Glacial development is related to both tectonics and climate conditions [51], and the difference in equilibrium lines between the Gongwang and Liangwang Mountains during the penultimate ice age, despite their similar tectonic and climatic conditions, suggests the involvement of other factors.

The Liangwang Mountains are surrounded by three highland lakes: Dianchi, Fuxian, and Yangzonghai. The influence of these lakes should not be overlooked, as they play a significant role in regional climate regulation. The presence of lakes leads to the formation of a regional lake climate, with the extent and depth of the lakes determining the degree of climate regulation [52,53]. Studies in the Kunming Basin reveal that around 12,000 ka B.P., during the time of glaciation in the Liangwang Mountains, the Dianchi Lake reached its peak size, which was nearly three times larger than its modern size. The Fuxian Lake also experienced unprecedented expansion, with the shoreline extending several kilometers to the north and south. These large lakes with extensive water surfaces absorb solar radiation, resulting in decreased reflectivity. Additionally, the large water bodies have a high specific heat and consume heat through evaporation, leading to moderate temperature changes in area around the Liangwang Mountains. Consequently, while the southeast region of the Qinghai–Tibet Plateau was cooling during the penultimate ice age, the area around the Liangwang Mountains maintained a stable and relatively low temperature conducive to glacier formation.

The glaciers in the Liangwangshan region developed significantly during the penultimate period glaciation, and this phenomenon was closely related to the climatic regulation role played by three large plateau lakes in the area. These lakes exchanged energy with their surrounding environment through their vast lake surfaces, thereby exerting a profound influence on the near-surface atmosphere. More importantly, the evaporation of water from the lakes significantly altered the precipitation distribution pattern in the Liangwangshan region. During winter and nighttime, the evaporation of water vapor from the lakes increases significantly, resulting in a notable increase in precipitation during these periods compared to modern levels [54,55]. In meteorological and glaciological studies, precipitation is a crucial factor in determining the theoretical equilibrium line—the altitude at which glacier accumulation and ablation reach a dynamic balance. Influenced by these

lakes, the theoretical equilibrium line in the Liangwangshan area is significantly lower than the 2800 m height predicted using conventional methods. This reduction provides the necessary climatic conditions for the formation and stable existence of glaciers at lower altitudes. Additionally, the temperature difference between the plateau lakes and the Liangwangshan terrain results in a significant lake–land breeze circulation phenomenon. At night, the land cools faster than the lakes, forming a land breeze blowing towards the lakes. Conversely, during the day, due to the lakes' large heat capacity, which causes a lag in warming, a lake breeze blows towards the land. This lake–land breeze circulation not only helps to regulate the temperature in the Liangwangshan area but also effectively lowers the surface temperature, especially during summer, thus creating favorable conditions for the formation and maintenance of glaciers.

In summary, we can conclude that there was a close correlation between the formation of the Liangwangshan glacier and the climatic regulation role of the three large plateau lakes. By altering precipitation patterns and generating lake–land breeze circulation, these lakes significantly impacted the climatic environment of the Liangwangshan region, thereby promoting the development of glaciers in the area during the penultimate period glaciation. Compared to Gongwangshan, which is located in the same geographical region, the lower altitude of the equilibrium line in Liangwangshan further supports the view that these lakes had a significant influence on glacier formation. Therefore, we believe that the formation of glaciers in the Liangwangshan region was closely related to the climatic regulation role of these plateau lakes.

5. Conclusions

This study provides evidence of glacial relics in the lower latitudes of the Liangwang Mountains on the southeastern Tibetan Plateau through the use of various analytical methods, including geomorphology, sedimentology, electron microscopy, spore analysis, and paleoclimatology. It is worth noting that these glacial relics represent the lowest-latitude glacial relic known in mainland China. Our fieldwork and indoor experimental analysis confirmed the existence of Quaternary glacial relics in the Liangwang Mountains. Additionally, we recovered the theoretical equilibrium line of the Liangwang Mountains and conducted a comparative analysis with the theoretical equilibrium line of typical glaciers. This analysis helped us to examine the possibility and timing of glacial development in the Liangwang Mountains based on the theoretical equilibrium line. Furthermore, we collected data on fir spore powder from boreholes in the Kunming Basin and compared them with the *Abies* content in the glacial sediments of the Liangwang Mountains. This comparison provided further confirmation of glacial development in the Liangwang Mountains during the penultimate ice age. Lastly, we compared the ice age history of the Liangwang Mountains with that of mountain glaciers in the southeastern Tibetan Plateau and discussed the influence of tectonics and climate on glacial development.

Our findings indicate that the lower equilibrium line of the Liangwang Mountains at this low latitude was not only influenced by significant cooling during the penultimate ice age, but also by the unique climatic effects of the three plateau lakes.

Author Contributions: Conceptualization, Y.P. and S.Z.; methodology, Y.P.; validation, Y.P., S.Z. and J.C.; formal analysis, Y.P.; investigation, Y.P.; resources, Y.P.; data curation, Y.P.; writing—original draft preparation, Y.P.; writing—review and editing, Y.P., S.Z., C.Z., J.C. and S.W.; visualization, Y.P.; supervision, Y.P., J.C., C.Z., S.Z. and S.W.; project administration, S.Z.; funding acquisition, S.Z. All authors have read and agreed to the published version of the manuscript.

Funding: This research is financially supported by the key international cooperation project of the National Natural Science Foundation of China, No. 42320104005, Evolution History of Plant Diversity in Yunnan Province during the Cenozoic Era and Its Key Driving Factors, 2024/01–2028/12; Youth Science Fund Project of the National Natural Science Foundation of China, Stratigraphic chronology and sporopollen assemblage characteristics of the late Paleogene strata in southeastern Yunnan, 42302030, 2024/01–2026/12.

Institutional Review Board Statement: Not applicable

Informed Consent Statement: Informed consent was obtained from all subjects involved in the study.

Data Availability Statement: The raw data supporting the conclusions of this article will be made available by the authors on request.

Acknowledgments: The authors are grateful for the helpful comments from many researchers and colleagues.

Conflicts of Interest: The authors declare no conflicts of interest.

References

1. Brook, E.J.; Buizert, C. Antarctic and global climate history viewed from ice cores. *Nature* **2018**, *558*, 200–208. [[CrossRef](#)] [[PubMed](#)]
2. Herbert, T.D. The Mid-Pleistocene Climate Transition. *Annu. Rev. Earth Planet. Sci.* **2023**, *51*, 389–418. [[CrossRef](#)]
3. Eaves, S.R.; Winckler, G.; Mackintosh, A.N.; Schaefer, J.M.; Townsend, D.B.; Doughty, A.M.; Jones, R.S.; Leonard, G.S. Late-glacial and Holocene glacier fluctuations in north island, New Zealand. *Quat. Sci. Rev.* **2019**, *223*, 105914. [[CrossRef](#)]
4. Lešić, N.-M.; Streuff, K.T.; Bohrmann, G.; Kuhn, G. Glacimarine sediments from outer Drygalski Trough, sub-Antarctic South Georgia—evidence for extensive glaciation during the Last Glacial Maximum. *Quat. Sci. Rev.* **2022**, *292*, 107657. [[CrossRef](#)]
5. Bolch, T.; Kulkarni, A.; Kääh, A.; Huggel, C.; Paul, F.; Cogley, J.G.; Frey, H.; Kargel, J.S.; Fujita, K.; Scheel, M. The state and fate of Himalayan glaciers. *Science* **2012**, *336*, 310–314. [[CrossRef](#)]
6. Shan, Z.; Li, Z.; Dong, X. Impact of glacier changes in the Himalayan Plateau disaster. *Ecol. Inform.* **2021**, *63*, 101316. [[CrossRef](#)]
7. Ehlers, T.A.; Chen, D.; Appel, E.; Bolch, T.; Chen, F.; Diekmann, B.; Dippold, M.A.; Giese, M.; Guggenberger, G.; Lai, H.-W. Past, present, and future geo-biosphere interactions on the Tibetan Plateau and implications for permafrost. *Earth-Sci. Rev.* **2022**, *234*, 104197. [[CrossRef](#)]
8. Lehmkuhl, F.; Owen, L.A. Late Quaternary glaciation of Tibet and the bordering mountains: A review. *Boreas* **2005**, *34*, 87–100. [[CrossRef](#)]
9. Owen, L.A.; Finkel, R.C.; Barnard, P.L.; Haizhou, M.; Asahi, K.; Caffee, M.W.; Derbyshire, E. Climatic and topographic controls on the style and timing of Late Quaternary glaciation throughout Tibet and the Himalaya defined by ^{10}Be cosmogenic radionuclide surface exposure dating. *Quat. Sci. Rev.* **2005**, *24*, 1391–1411. [[CrossRef](#)]
10. Zhou, S.; Xu, L.; Colgan, P.M.; Mickelson, D.M.; Wang, X.; Wang, J.; Zhong, W. Cosmogenic ^{10}Be dating of Guxiang and Baiyu glaciations. *Chin. Sci. Bull.* **2007**, *52*, 1387–1393. [[CrossRef](#)]
11. Thompson, L.o.; Yao, T.; Davis, M.; Henderson, K.; Mosley-Thompson, E.; Lin, P.-N.; Beer, J.; Synal, H.-A.; Cole-Dai, J.; Bolzan, J. Tropical climate instability: The last glacial cycle from a Qinghai-Tibetan ice core. *Science* **1997**, *276*, 1821–1825. [[CrossRef](#)]
12. Chen, R.; Zhou, S.; Li, Y.; Lai, Z.; Ou, X.; Lu, X.; Li, Y. Late Quaternary climate and environmental change derived from glacial deposits in the Parlung Zangbo Valley, southeastern Tibetan Plateau. *Phys. Geogr.* **2020**, *41*, 99–125. [[CrossRef](#)]
13. Li, K.; Liu, X.; Herzsuh, U.; Wang, Y. Rapid climate fluctuations over the past millennium: Evidence from a lacustrine record of Basomtso Lake, southeastern Tibetan Plateau. *Sci. Rep.* **2016**, *6*, 24806. [[CrossRef](#)]
14. Wang, X.; Chai, K.; Liu, S.; Wei, J.; Jiang, Z.; Liu, Q. Changes of glaciers and glacial lakes implying corridor-barrier effects and climate change in the Hengduan Shan, southeastern Tibetan Plateau. *J. Glaciol.* **2017**, *63*, 535–542. [[CrossRef](#)]
15. Chen, R.; Zhou, S.; Lai, Z.; Ou, X.; Chen, R.; Deng, Y. Luminescence chronology of late Quaternary moraines and Last Glacial Maximum equilibrium-line altitude reconstruction from Parlung Zangbo Valley, south-eastern Tibetan Plateau. *J. Quat. Sci.* **2014**, *29*, 597–604. [[CrossRef](#)]
16. Chen, Y.; Li, Y.; Zhang, M.; Cui, Z.; Liu, G. Much late onset of Quaternary glaciations on the Tibetan Plateau: Determining the age of the Shishapangma Glaciation using cosmogenic ^{26}Al and ^{10}Be dating. *Sci. Bull.* **2018**, *63*, 306–313. [[CrossRef](#)]
17. Zheng, B.; Xu, Q.; Shen, Y. The relationship between climate change and Quaternary glacial cycles on the Qinghai–Tibetan Plateau: Review and speculation. *Quat. Int.* **2002**, *97*, 93–101. [[CrossRef](#)]
18. Wang, M.; Wang, X.; Pan, B.; Yi, S.; Van Balen, R.; Zhao, Z.; Dong, X.; Vandenberghe, J.; Wang, Y.; Lu, H. Multiple paleolakes caused by glacier river-blocking on the southeastern Tibetan plateau in response to climate changes since the last glacial maximum. *Quat. Sci. Rev.* **2023**, *305*, 108012. [[CrossRef](#)]
19. Yang, J.; Zhang, W.; Cui, Z.; Yi, C.; Liu, K.; Ju, Y.; Zhang, X. Late Pleistocene glaciation of the Diancang and Gongwang Mountains, southeast margin of the Tibetan Plateau. *Quat. Int.* **2006**, *154*, 52–62. [[CrossRef](#)]
20. Zhang, W.; Chai, L.; Evans, I.S.; Liu, L.; Li, Y.-P.; Qiao, J.-R.; Tang, Q.-Y.; Sun, B. Geomorphic features of Quaternary glaciation in the Taniantaweng Mountain, on the southeastern Qinghai-Tibet Plateau. *J. Mt. Sci.* **2019**, *16*, 256–274. [[CrossRef](#)]
21. Ruiz-Fernández, J.; Oliva, M.; Hughes, P. Permafrost and periglacial processes in mid-and low-latitude mountain regions. *Permafr. Periglac. Process.* **2019**, *30*, 245–248. [[CrossRef](#)]
22. Chandler, B.M.; Lovell, H.; Boston, C.M.; Lukas, S.; Barr, I.D.; Benediktsson, Í.Ö.; Benn, D.I.; Clark, C.D.; Darvill, C.M.; Evans, D.J. Glacial geomorphological mapping: A review of approaches and frameworks for best practice. *Earth-Sci. Rev.* **2018**, *185*, 806–846. [[CrossRef](#)]
23. Chmielowska, D.; Woronko, B.; Dorocki, S. Applicability of automatic image analysis in quartz-grain shape discrimination for sedimentary setting reconstruction. *CATENA* **2021**, *207*, 105602. [[CrossRef](#)]

24. Itamiya, H.; Sugita, R.; Sugai, T. Analysis of the surface microtextures and morphologies of beach quartz grains in Japan and implications for provenance research. *Prog. Earth Planet. Sci.* **2019**, *6*, 43. [\[CrossRef\]](#)
25. Vos, K.; Vandenbergh, N.; Elsen, J. Surface textural analysis of quartz grains by scanning electron microscopy (SEM): From sample preparation to environmental interpretation. *Earth-Sci. Rev.* **2014**, *128*, 93–104. [\[CrossRef\]](#)
26. Woronko, B.; Dłużewski, M.; Woronko, D. Sand-grain micromorphology used as a sediment-source indicator for Kharga Depression dunes (Western Desert, S Egypt). *Aeolian Res.* **2017**, *29*, 42–54. [\[CrossRef\]](#)
27. Woronko, B. Frost weathering versus glacial grinding in the micromorphology of quartz sand grains: Processes and geological implications. *Sediment. Geol.* **2016**, *335*, 103–119. [\[CrossRef\]](#)
28. Chmielowska, D.; Woronko, B. A source of loess-like deposits and their attendant palaeoenvironment—Orava Basin, Western Carpathian Mountains, S Poland. *Aeolian Res.* **2019**, *38*, 60–76. [\[CrossRef\]](#)
29. Kalińska, E.; Lamsters, K.; Karušs, J.; Krievāns, M.; Rečs, A.; Ješkins, J. Does glacial environment produce glacial mineral grains? Pro- and supra-glacial Icelandic sediments in microtextural study. *Quat. Int.* **2022**, *617*, 101–111. [\[CrossRef\]](#)
30. Wang, W.-X.; Zhao, X.-L.; Li, S.-J.; Zhang, L.; Wang, X.-L.; Zhang, X.-Y. Palynoflora and climatic dynamics of the Laizhou Bay of Bohai Sea, North China Plain, since the late middle Pleistocene. *J. Palaeogeogr.* **2023**, *12*, 278–295. [\[CrossRef\]](#)
31. Wu, F.; Miao, Y.; Meng, Q.; Fang, X.; Sun, J. Late Oligocene Tibetan Plateau warming and humidity: Evidence from a sporopollen record. *Geochem. Geophys. Geosyst.* **2019**, *20*, 434–441. [\[CrossRef\]](#)
32. Ohmura, A.; Kasser, P.; Funk, M. Climate at the equilibrium line of glaciers. *J. Glaciol.* **1992**, *38*, 397–411. [\[CrossRef\]](#)
33. Shi, Y. *Glaciations and Environmental Variations in East China*; Science Press: Beijing, China, 1989.
34. Zhang, W.; Li, Y.; Liu, B. Development and Cause of Glacial since Middle Pleistocene in Low Latitude of China. *Geogr. Geo-Inf. Sci.* **2013**, *29*, 78–83.
35. Kuang, M.; Li, J.; Zhao, Y. Quaternary glacial remains in Gongwang Mountain, Northeastern Yunnan Province. *J. Glaciol. Geocryol.* **1997**, *19*, 78–84.
36. Zhang, W.; Cui, Z.; Feng, J.; Yi, C.; Yang, J. Late Pleistocene glaciation of the Hulifang massif of Gongwang mountains in Yunnan Province. *J. Geogr. Sci.* **2005**, *15*, 448–458. [\[CrossRef\]](#)
37. Wang, L.; Chen, R.; Song, Y.; Yang, Y.; Liu, J.; Han, C.; Liu, Z. Precipitation–altitude relationships on different timescales and at different precipitation magnitudes in the Qilian Mountains. *Theor. Appl. Climatol.* **2018**, *134*, 875–884. [\[CrossRef\]](#)
38. Fu, P.; Stroeve, A.P.; Harbor, J.M.; Hättstrand, C.; Heyman, J.; Caffee, M.W.; Zhou, L. Paleoglaciology of Shaluli Shan, southeastern Tibetan plateau. *Quat. Sci. Rev.* **2013**, *64*, 121–135. [\[CrossRef\]](#)
39. Zhao, Y.; Tzedakis, P.C.; Li, Q.; Qin, F.; Cui, Q.; Liang, C.; Birks, H.J.B.; Liu, Y.; Zhang, Z.; Ge, J. Evolution of vegetation and climate variability on the Tibetan Plateau over the past 1.74 million years. *Sci. Adv.* **2020**, *6*, eaay6193. [\[CrossRef\]](#) [\[PubMed\]](#)
40. Tong, G.; Bai, T.; Zhou, S. Fluctuating characteristics of Quaternary sporulation time series in the Kunming Basin and their geo-environmental significance. *J. Integr. Plant Biol.* **1990**, *32*, 146–156.
41. Xu, L.; Zhou, S. Quaternary glaciations recorded by glacial and fluvial landforms in the Shaluli Mountains, Southeastern Tibetan Plateau. *Geomorphology* **2009**, *103*, 268–275. [\[CrossRef\]](#)
42. Zhang, Q.; Yi, C.; Dong, G.; Fu, P.; Wang, N.; Capolongo, D. Quaternary glaciations in the lopu kangri area, central Gangdise mountains, southern Tibetan plateau. *Quat. Sci. Rev.* **2018**, *201*, 470–482. [\[CrossRef\]](#)
43. He, J.; Wang, J.; Zheng, C.; Li, W.; Sun, W.; Guo, T.; Zeng, S. Geochemical characteristics of lake clay drilled in well QZ-4: Its implication for geochemical response to climate change in the central Tibetan Plateau in the Middle–Late Pleistocene. *Environ. Earth Sci.* **2016**, *75*, 1312. [\[CrossRef\]](#)
44. Zhang, W.; Liu, L.; Chai, L.; He, D. Characteristics of quaternary glaciations using ESR dating method in the luoji mountain, sichuan province. *Quat. Sci.* **2017**, *37*, 281–292.
45. Chen, A.; Zheng, M.; Shi, L.; Wang, H.; Xu, J. Magnetostratigraphy of deep drilling core 15YZK01 in the northwestern Qaidam Basin (NE Tibetan Plateau): Tectonic movement, salt deposits and their link to Quaternary glaciation. *Quat. Int.* **2017**, *436*, 201–211. [\[CrossRef\]](#)
46. Liu, X.; Xu, Q.; Ding, L. Differential surface uplift: Cenozoic paleoelevation history of the Tibetan Plateau. *Sci. China Earth Sci.* **2016**, *59*, 2105–2120. [\[CrossRef\]](#)
47. Xiang, F.; Huang, H.; Ogg, J.G.; Zhu, H.; Kang, D. Quaternary sediment characteristics and paleoclimate implications of deposits in the Three Gorges and Yichang areas of the Yangtze River. *Geomorphology* **2020**, *351*, 106981. [\[CrossRef\]](#)
48. Shi, X.-h.; Wang, E.; Wang, G.; Fan, C. Late cenozoic uplift of the yulong snow mountain (5596 m), se tibetan plateau, caused by erosion and tectonic forcing. *Quat Sci* **2008**, *28*, 222–231.
49. Li, B.-L.; Ji, J.-Q.; Lo, C.-H.; Gong, J.-F.; Qing, J.-C. The structural style and timing of uplift of the Ailaoshan-Diancang Range, West Yunnan, China. *Dizhen Dizhi* **2012**, *34*, 696–712.
50. Wang, J.; Raisbeck, G.; Xu, X.; Yiou, F.; Bai, S. In situ cosmogenic ¹⁰Be dating of the Quaternary glaciations in the southern Shaluli Mountain on the Southeastern Tibetan Plateau. *Sci. China Ser. D Earth Sci.* **2006**, *49*, 1291–1298. [\[CrossRef\]](#)
51. Riechers, K.; Mitsui, T.; Boers, N.; Ghil, M. Orbital insolation variations, intrinsic climate variability, and Quaternary glaciations. *Clim. Past* **2022**, *18*, 863–893. [\[CrossRef\]](#)
52. Martynov, A.; Sushama, L.; Laprise, R.; Winger, K.; Dugas, B. Interactive lakes in the Canadian Regional Climate Model, version 5: The role of lakes in the regional climate of North America. *Tellus A Dyn. Meteorol. Oceanogr.* **2012**, *64*, 16226. [\[CrossRef\]](#)

53. Zhu, L.; Jin, J.; Liu, X.; Tian, L.; Zhang, Q. Simulations of the impact of lakes on local and regional climate over the Tibetan Plateau. *Atmosphere-Ocean* **2018**, *56*, 230–239. [[CrossRef](#)]
54. Dai, Y.; Yao, T.; Wang, L.; Li, X.; Zhang, X. Contrasting roles of a large alpine lake on tibetan plateau in shaping regional precipitation during summer and autumn. *Front. Earth Sci.* **2020**, *8*, 358. [[CrossRef](#)]
55. Specht, N.F.; Claussen, M.; Kleinen, T. Dynamic interaction of lakes, climate and vegetation over northern Africa during the mid-Holocene. *EGUsphere* **2024**, *2024*, 1–27.

Disclaimer/Publisher’s Note: The statements, opinions and data contained in all publications are solely those of the individual author(s) and contributor(s) and not of MDPI and/or the editor(s). MDPI and/or the editor(s) disclaim responsibility for any injury to people or property resulting from any ideas, methods, instructions or products referred to in the content.